JVST A
Journal of Vacuum Science & Technology A

Formation and desorption of nickel hexafluoroacetylacetonate $Ni(hfac)_2$ on a nickel oxide surface in atomic layer etching processes

Cite as: J. Vac. Sci. Technol. A **38**, 052602 (2020); https://doi.org/10.1116/6.0000293
Submitted: 04 May 2020 . Accepted: 17 July 2020 . Published Online: 06 August 2020

Abdulrahman H. Basher, Marjan Krstić, Karin Fink, Tomoko Ito, Kazuhiro Karahashi, Wolfgang Wenzel, and Satoshi Hamaguchi

JVST A
Journal of Vacuum Science & Technology A

ARTICLE

avs.scitation.org/journal/jva

Formation and desorption of nickel hexafluoroacetylacetonate $Ni(hfac)_2$ on a nickel oxide surface in atomic layer etching processes

Cite as: J. Vac. Sci. Technol. A 38, 052602 (2020); doi: 10.1116/6.0000293
Submitted: 4 May 2020 · Accepted: 17 July 2020 ·
Published Online: 6 August 2020

Abdulrahman H. Basher,[1,a)] Marjan Krstić,[2] Karin Fink,[3] Tomoko Ito,[1] Kazuhiro Karahashi,[1] Wolfgang Wenzel,[2] and Satoshi Hamaguchi[1,b)]

AFFILIATIONS

[1]Center for Atomic and Molecular Technologies, Osaka University, 2-1 Yamadaoka, Suita, Osaka 565-0871, Japan
[2]3DMM2O—Cluster of Excellence (EXC-2082/1–390761711), Institute of Nanotechnology, Karlsruhe Institute of Technology (KIT), Hermann-von-Helmholtz-Platz 1, 76344 Eggenstein-Leopoldshafen, Germany
[3]Institute of Nanotechnology, Karlsruhe Institute of Technology (KIT), Hermann-von-Helmholtz-Platz 1, 76344 Eggenstein-Leopoldshafen, Germany

Note: This paper is part of the Special Topic Collection Commemorating the Career of John Coburn.
[a)]**Electronic mail:** a.h.basher@ppl.eng.osaka-u.ac.jp
[b)]**Electronic mail:** hamaguch@ppl.eng.osaka-u.ac.jp

ABSTRACT

Thermal atomic layer etching (ALE) of nickel (Ni) may be performed with a step of thin-layer oxidation of its surface and another step of its removal by gas-phase hexafluoroacetylacetone (hfacH) as an etchant. In this study, adsorption of hfacH and possible formation of volatile nickel hexafluoroacetylacetonate $Ni(hfac)_2$ on a NiO surface were investigated based on the density functional theory (DFT) with more realistic surface material models than those used in the previous study [A. H. Basher *et al.*, J. Vac. Sci. Technol. A **38**, 022610 (2020)]. It has been confirmed that an hfacH molecule approaching a NiO surface deprotonates without a potential barrier and adsorbs on the surface exothermically. In addition, stable adsorption of two deprotonated hfacH molecules on a NiO (100) surface was found to occur not on a single Ni atom but over a few Ni atoms instead, which makes the formation of a $Ni(hfac)_2$ complex on the flat surface very unlikely even at elevated temperature. However, if the surface is rough and a Ni atom protrudes from the surrounding atoms, two hexafluoroacetylacetonate anions ($hfac^-$) can bond to the Ni atom stably, which suggests a possibility of desorption of a $Ni(hfac)_2$ complex from the surface at elevated temperature. Given the experimentally observed fact that desorption of $Ni(hfac)_2$ complexes typically takes place on a NiO surface at a temperature of ~300–400 °C, our DFT calculations indicate that the surface roughness of an oxidized Ni surface facilitates the formation and desorption of organometallic complexes $Ni(hfac)_2$, and therefore, the resulting Ni surface after ALE can be smoother than the initial surface.

I. INTRODUCTION

Atomic layer etching (ALE) is a technique to etch materials layer by layer in a controlled manner, typically repeating a cycle of a surface modification step and a step to remove the surface layer affected by the preceding step.[1–7] In ALE, at least one of the steps must be self-limiting in a sense that the surface modification or the removal step ends automatically without a temporal adjustment of process conditions.[8–11] Although various ALE techniques were invented decades ago to form extremely small structures on a material surface,[12–17] their practical importance has grown rapidly in recent years as they have been applied for manufacturing of semiconductor devices whose dimensions are approaching the atomic scale.[7,10,18–20]

ALE processes may be divided into two categories: plasma-assisted ALE[4,9,10,19,20] and thermal ALE.[10,18,20–22] In a

typical plasma-assisted ALE, a modified surface layer is removed by the impact of low-energy plasma-generated ions incident upon the surface. The surface modification may also be performed with free radicals generated by chemically reactive plasmas. The kinetic energy of the incident ions is set sufficiently low so that the etching process automatically stops once the chemically modified surface layer is completely removed. The major advantages of plasma-assisted ALE are that etching can be performed at low surface temperature, and anisotropic etching can be achieved owing to the directionality of incident ion motion. A possible disadvantage of plasma-assisted ALE is that ion bombardment may cause atomic-scale surface damages even at low ion incident energy.[2–4,9,10]

In a typical thermal ALE, a modified surface is removed by chemical reactions that form volatile molecules. The removal process is self-limiting because the surface chemical reactions are designed not to proceed further once the modified surface is completely removed. The major advantages of thermal ALE are that the process hardly leaves any damage to the surface, and isotropic etching can be achieved because the surface reactions are typically non-directional. Its possible disadvantage is that it requires an elevated surface temperature to promote the surface reactions for desorption.[1,5,8,11,18,21–25]

The motivation of this study comes from our interest in developing damageless etching technologies for magnetic metals such as Co, Fe, and Ni, which are typically used as materials for magnetic tunnel junctions (MTJs) in magnetoresistive random access memories (MRAMs). One of the major obstacles for the development of highly integrated MRAMs is the miniaturization of an MTJ, which consists of multiple thin layers of ferromagnetic metals and an insulating tunneling barrier layer.[19] As the dimensions of MTJ cells decrease, damages incurred by the ion impact of Ar ion milling or plasma etching in the manufacturing process of MTJ cells degrade their functionality, which prevent further miniaturization of MRAMs. Therefore, the use of damageless thermal etching is an attractive alternative for MTJ manufacturing processes.

Thermal ALE of the metal may be performed in the following manner: a top thin layer of the metal surface is either oxidized or halogenated first (the surface modification step) and then the oxidized/halogenated surface is exposed to organic molecules at an elevated surface temperature. In the latter step, volatile organometallic complexes form and remove metal atoms from the oxidized/halogenated metal surface (the removal step). The etching stops when the oxidized/halogenated layer is exhausted in the removal step because such organic molecules typically do not react with pure metallic surfaces.[11,12,23,24,26] For example, in the case of thermal ALE of metallic Ni, first the Ni film may be exposed to an oxygen plasma to form a thin nickel oxide (NiO) layer, i.e.,

$$\mathrm{Ni} + \mathrm{O} \rightarrow \mathrm{NiO}.$$

This is the surface modification step. In the removal step, the NiO surface is exposed to gaseous hexafluoroacetylacetone (hfacH) at a surface temperature of ~300–400 °C. Then, volatile nickel hexafluoroacetylacetonate $\mathrm{Ni(hfac)_2}$ complexes and water molecules $\mathrm{H_2O}$ are formed and desorbed from the surface through the reaction

$$\mathrm{NiO} + 2\mathrm{hfacH} \rightarrow \mathrm{Ni(hfac)_2} + \mathrm{H_2O}.$$

In this way, one can remove the oxidized layer formed on the Ni film. It is known that the desorption of $\mathrm{Ni(hfac)_2}$ does not take place on a metallic Ni surface.[1,20,24]

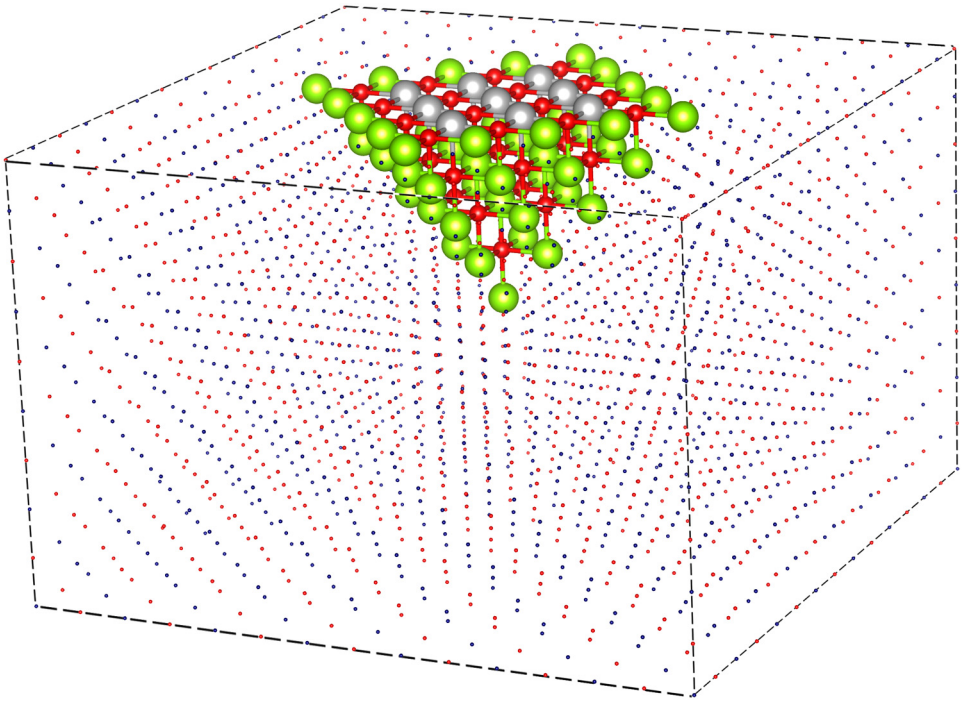

FIG. 1. Atomic configurations of the NiO four shell surface material model used in our DFT calculations. All atoms are in the lattice sites of the rectangular NiO crystalline structure with a dimension of 29.33 × 29.33 × 18.86 Å^3, having a (100) top surface. It consists of the QM region, represented by the collection of gray, red, and green spheres located near the center of the top surface and the embedding region represented by the blue and red dots occupying the NiO lattice sites outside the QM region. All calculations were performed for this rectangular box in the presence of the embedding region with different models of the QM region. Here, gray, red, and green spheres represent Ni, O, and Mg atoms, respectively, and blue and red dots represent PCs. For details, the reader is referred to the main text.

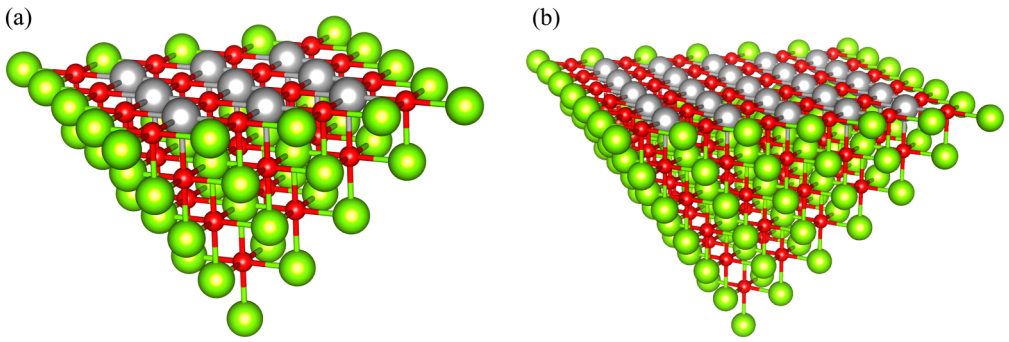

FIG. 2. Optimized structures of the (a) "four shell model" and (b) "six shell model" of the QM region having a NiO (100) surface, whose arrangement of atoms is given in Table I.

Several organic molecules have been tested with Ni and other metals for thermal ALE processes experimentally.[23,24,26] For instance, Chen *et al.*[27,28] performed ALE of Fe, Cu, Co, Pd, Pt, and CoPt with a wet chemical etch by acetylacetone (acacH), hfacH, ethylenediaminetetraacetic acid (edta), nitrilotriacetic acid (nta), pyridine-2,6-dicarboxylic acid (pdca), oxalic acid (oa), and formic acid (fa). Zhao *et al.* investigated thermal dry ALD of Co by oxidation and hfacH-based desorption,[23] and Konh *et al.* studied thermal dry ALE of Co by chlorination and hfacH/acacH-based desorption.[26] Dry thermal ALE of Ni and Co by oxidation and hfacH/acacH-based desorption was also demonstrated by Ito *et al.*[24]

In this study, focusing on thermal ALE of metallic Ni by oxidation and hfacH exposure, we have examined the surface reaction mechanisms of an oxidized Ni surface exposed to gaseous hfacH molecules, using first-principles quantum mechanical (QM) calculations. The recent study of Basher *et al.*[1] evaluated the reaction energies of adsorption processes of hfacH on metallic Ni and NiO surfaces, using QM calculations based on the density functional theory (DFT). However, the model surfaces used in their study were simple monolayers to minimize the computational complexity. One of the goals of this study is, therefore, to re-evaluate the previously reported values of reaction energies of hfacH adsorption on a NiO surface with more realistic multilayer surface material models. Another goal is to understand the mechanisms of the formation of nickel hexafluoroacetylacetonate $Ni(hfac)_2$ complexes on a NiO surface and their desorption. The formation and desorption processes were not discussed in Ref. 1 and, therefore, are the main focus of this study.

Instead of using just thermal energy to form organometallic complexes, ligand exchange reactions among several organometallic complexes can also be used to perform thermal ALE.[5] Reaction mechanisms of such thermal ALE are out of the scope of this study.

II. MODELING

All QM calculations in this study were performed with TURBOMOLE V7.3.1[29] software based on a DFT method with Gaussian type atomic orbitals. As in Refs. 30 and 31, where ZnO

TABLE I. Information on atomic configurations in the QM regions of two NiO surface material models used in this study. In the "Coordinates" column, "Fixed" indicates that the atoms listed in the same row are set immobile during structural optimization.

		QM region	Numbers	Coordinates
Four shell model	Central	Ni	1	
	1st Shell	O	5	
	2nd Shell	Ni, Mg	8, 5	Fixed
	3rd Shell	O	25	
	4th Shell	Mg	41	Fixed and treated as ECP
	PCs		2165	Fixed
Six shell model	Central	Ni	1	
	1st Shell	O	5	
	2nd Shell	Ni, Mg	8, 5	Fixed
	3rd Shell	O	25	
	4th Shell	Ni, Mg	16, 25	Fixed
	5th Shell	O	61	
	6th Shell	Mg	85	Fixed and treated as ECP
	PCs		2019	Fixed

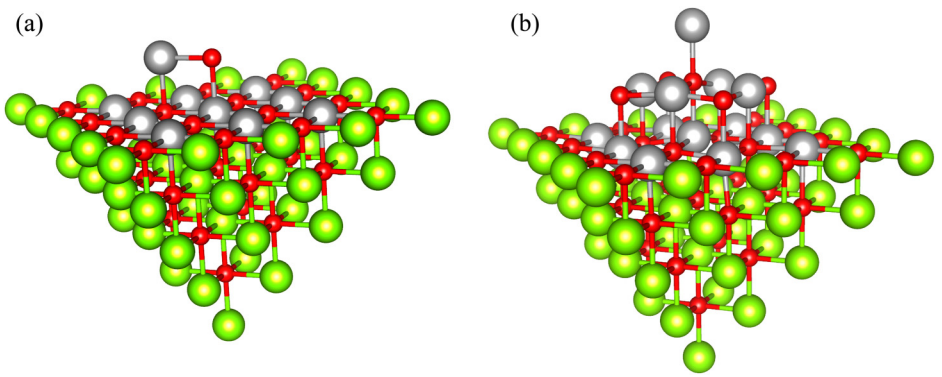

FIG. 3. Optimized structures of rough surface models with (a) Ni and O atoms added to the surface of the four shell model and (b) 5 Ni and 5 O atoms arranged in a pyramidlike structure added to the four shell model.

surfaces were modeled with the embedded cluster method (ECM),[30,31] we constructed a multilayer material model representing crystalline NiO with its (100) surface, using the ECM. Figure 1 shows the entire model system (which we call the ECM model) representing a NiO material used in this study. Here, the colored spheres represent atoms in our DFT calculations, whereas the colored dots represent point charges (PCs) that provide the electrostatic field to the DFT calculation region.

To reduce the computational load without much affecting the physical processes of adsorption, we replaced Ni atoms of lower and outermost layers with Mg atoms while keeping Ni atoms on the top surface that can directly interact with adsorbing molecules. This is because Mg has fewer electrons than Ni, while Ni and Mg have similar valence electron structures and both NiO and MgO have the halite (i.e., rock salt or NaCl) structure with similar lattice constants.[32,33]

In Fig. 1, the gray, red, and green spheres represent Ni, O, and Mg atoms, respectively, and small blue and red dots represent positive ($+2e$) and negative ($-2e$) PCs with e being the elementary charge. The model material has the halite (cubic) structure with a lattice constant of NiO, i.e., 4.19 Å.[34–37] The dimensions of the rectangular cube shown in Fig. 1 are $29.33 \times 29.33 \times 18.86$ Å^3 and the top surface represents a (100) surface. In this ECM model, we call the region where atoms are represented by spheres in Fig. 1, the QM region and the rest of the embedding region. In the QM region, all atoms except for those in the outermost layer are treated quantum mechanically during DFT calculations, as will be explained more in detail momentarily. In this study, adsorbed hfacH molecules are set to interact only with the NiO top surface of this model, keeping sufficient distance from surrounding Mg atoms, so we believe that the interaction of hfacH with a NiO (100) surface can be well represented with this model material.

Figure 2(a) shows the QM region of Fig. 1. This region was formed in the following manner: First, we placed a single Ni atom. This atom corresponds to the one located at the center of the top surface of Fig. 2(a). Note that if this Ni atom were in the bulk, six O atoms should occupy the first octahedral shell surrounding it. Second, to create a NiO (100) surface with this Ni atom being in the center, we placed five O atoms (excluding the O atom just above the Ni atom) in the octahedral shell around the Ni atom,

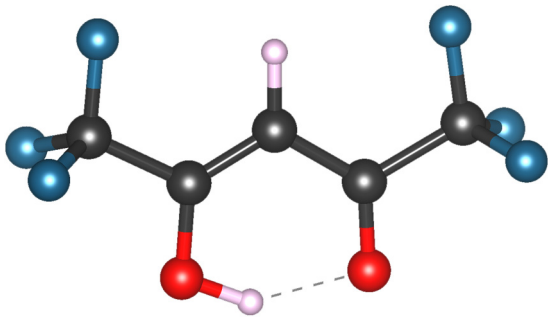

FIG. 4. Optimized structure of an enol-type hfacH molecule. Here, dark gray, red, blue, and white spheres represent C, O, F, and H atoms, respectively.

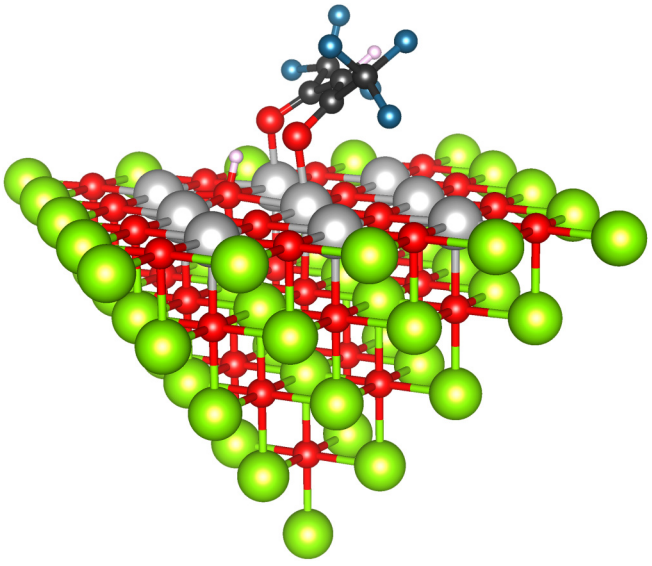

FIG. 5. Optimized structure of the four shell model for a NiO (100) surface with an adsorbed hfacH molecule after deprotonation.

TABLE II. Reaction energies of Fig. 5 for the adsorption of a single hfacH on a NiO (100) surface, evaluated with different functionals and assumptions of the dispersion effects.

Functionals	PBE (eV)	PBE0 (eV)	B3LYP (eV)
With D3-BJ	−2.26	−2.36	−2.45
Without D3-BJ	−1.55	−1.59	−1.47

with four of them together with the Ni atom forming a plane [the (100) surface] and another O atom being just below the Ni atom, as seen in Fig. 2(a). These five O atoms form the first shell of the model material. We then placed 13 metal atoms in the second shell surrounding the first shell, excluding the region above the (100) surface. Among the 13 metal atoms, eight of them occupying the same (100) surface were Ni atoms and the other five (below the top surface) were Mg atoms. Similarly, we formed the third shell consisting of 25 O atoms. In the fourth shell, all 41 metal atoms on or below the (100) surface were Mg atoms. As seen in Fig. 2(a), the outermost edge of the flat (100) surface in the QM region consists of 16 Mg atoms. We call this model material the NiO four shell model. The shell structures and the number of atoms in each shell are summarized in Table I.

As seen in Fig. 1, in the embedding region, the positive and negative PCs occupy the lattice sites of Ni and O atoms. The total number of PCs in this model is 2165. Our DFT calculations were performed for atoms in the QM region with the electric field produced by the immobile PCs (i.e., the positions of all PCs were fixed during the calculations) to include the influence of far ionic atoms of the bulk material. In what follows, all DFT calculations are performed in the presence of the PC electric field even when the figure shows only the QM region without PCs.

For some calculations, we used an extended shell model, as shown in Fig. 2(b). It is in the shape of an inverse square pyramid (i.e., the bottom half of an octahedron) similar to Fig. 2(a) with additional O and Mg shells. The outermost shell is the sixth shell that consists only of Mg atoms. We call this model system the NiO six shell model. The number of atoms in each shell is also summarized in Table I. It consists of 25 Ni atoms on the top (100) surface. The QM region of the NiO six shell model is embedded in the same NiO rectangular box of Fig. 1, which makes the number of PCs 2019.

No periodic boundary condition is imposed on the surface material model in this study. The embedding region has no global dipole moment arising from the PCs because each plane boundary surface of the rectangular box consists of the same number of positive and negative charges, i.e., carries no net charge. Therefore, unlike the ECM of ZnO in Refs. 30 and 31, no counter charge needs to be added to this system.

In our DFT calculations, we employed generalized gradient approximation Perdew–Burke–Ernzerhof (PBE) functionals.[38–41] As to the basis sets, we employed def2-SVP[42] for Ni and Mg atoms, except for Mg atoms in the outermost shell, and def2-TZVP[43] for all O atoms of the surface material model as well as all atoms of hfacH. Furthermore, the Grimme's D3 dispersion corrections[44,45] with Becke-Johnson (BJ)[46] damping were used to represent London dispersion forces (or what are loosely called van der Waals forces).

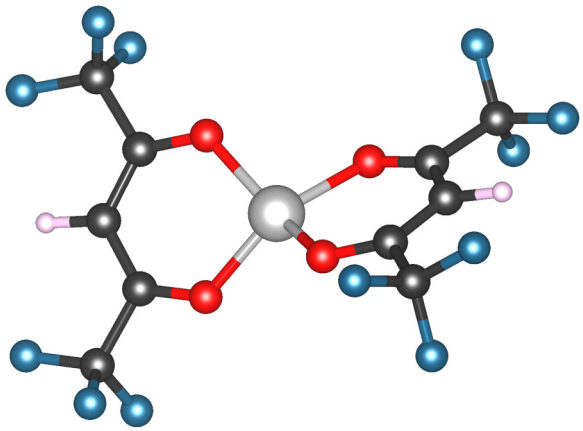

FIG. 6. Optimized structure of a $Ni(hfac)_2$ complex. Here, dark gray, red, blue, and white spheres represent Ni, O, F, and H atoms, respectively.

Each Mg atom in the outermost shell was approximated by the effective core potential (ECP) of ecp-10-sdf[47] as well as $-2e$ fixed charge and served as an additional embedding potential to prevent leakage of the electron density of the negatively charged O atoms. In other words, the Mg atoms in the outermost shell of the QM region were not evaluated quantum mechanically.

All geometries were fully optimized using gradient minimization techniques with the resolution of the Identity approximation for the Coulomb energy (RI-J)[48,49] and multipole accelerated RI-J (MARIJ)[50] option as implemented in TURBOMOLE 7.3.1 code.[29]

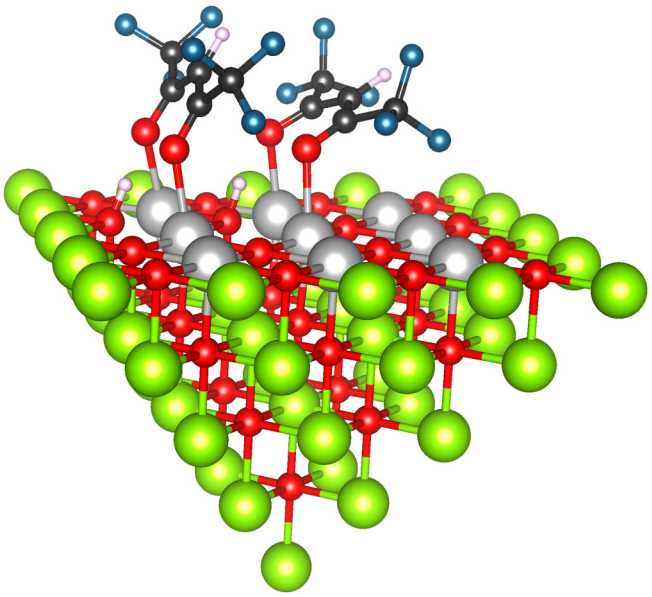

FIG. 7. Optimized structure of the four shell model for a NiO (100) surface with two adsorbed hfacH molecules after deprotonation.

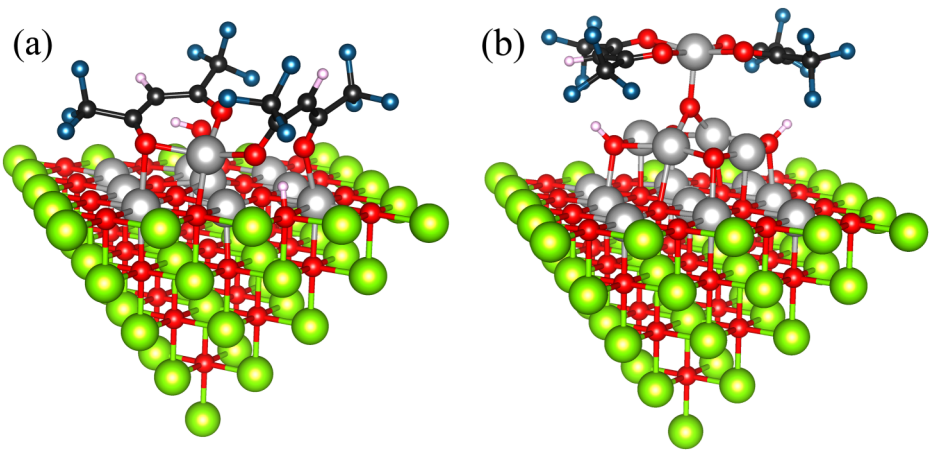

FIG. 8. Optimized structures of the rough surface models of (a) Figs. 3(a) and 3(b) with two adsorbed hfacH molecules after deprotonation. In each surface, a Ni(hfac)$_2$-like structure is formed around the topmost Ni atom.

The structural optimization of the QM region of the surface material model was performed in the following manner: The positions of all Mg atoms and PCs were set immobile, and the positions of all Ni and O atoms were optimized to achieve the lowest total energy of the system. The QM regions given in Figs. 2(a) and 2(b) are depicted after converged structural optimizations.

As a model of a non-smooth or "rough" surface, we placed single Ni and O atoms just above the surface O and Ni atoms and performed structural optimization, as shown in Fig. 3(a). Here, the added O atom was placed above the Ni atom at the center of the surface area and the added Ni atom was placed above one of the surface O atoms in the first shell.

Another model of a rough surface was formed with five additional NiO units stacked on the NiO surface, as shown in Fig. 3(b). Here, the NiO structure was formed by extending the first and third octahedral shells of O atoms up to the first monolayer above the original (100) surface of Fig. 2(a) and completing the second octahedral shell of Ni atoms above the (100) surface. Figure 3(b) shows this rough surface model after DFT structural optimization.

As to an hfacH molecule, the enol form is known to be more stable than the keto form.[1,51–55] Therefore, we only use the enol form of hfacH, as shown in Fig. 4. Here, dark gray, blue, and white spheres represent carbon (C), fluorine (F), and hydrogen (H) atoms, respectively.

III. RESULTS AND DISCUSSION

First, we evaluate the reaction energy of hfacH adsorption on a NiO surface. The reaction energy of a surface-molecule interaction is defined in general as

$$\text{Reaction energy} = E_{\text{total}} - E_{\text{ad}} - E_{\text{surf}}, \tag{1}$$

where E_{total} is the total energy of the system with (a) molecule(s) adsorbed on a NiO model surface, E_{ad} is the total energy of the

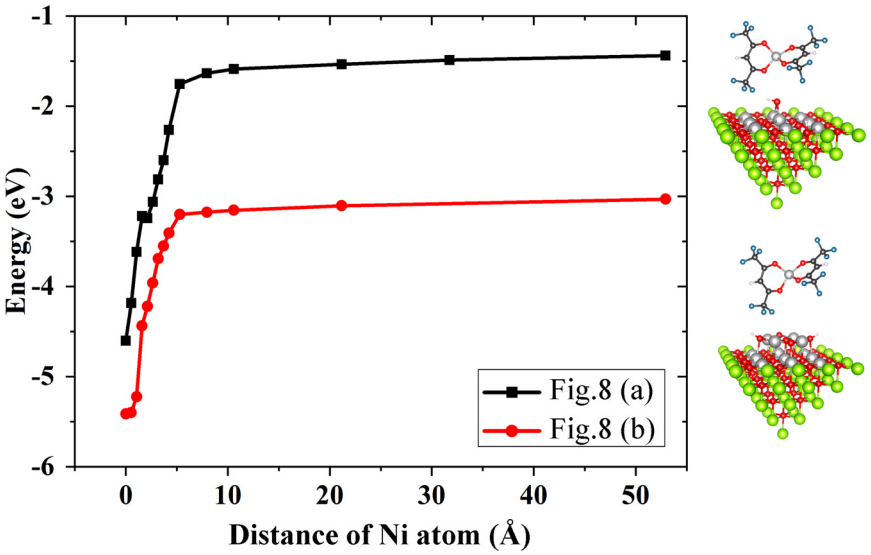

FIG. 9. System energy as a function of the position of the topmost Ni when two hfacH molecules are adsorbed around the protruding Ni atom of a rough surface. The black and red curves represent the cases of Figs. 8(a) and 8(b). The abscissa represents the distance of the Ni atom measured from its initial position given in Fig. 8 in each case. The ordinate represents the change in energy measured from the initial system energy prior to adsorption, i.e., the total energy of the system consisting of the surface material model of Fig. 3 and two hfacH molecules of Fig. 4 away from the surface.

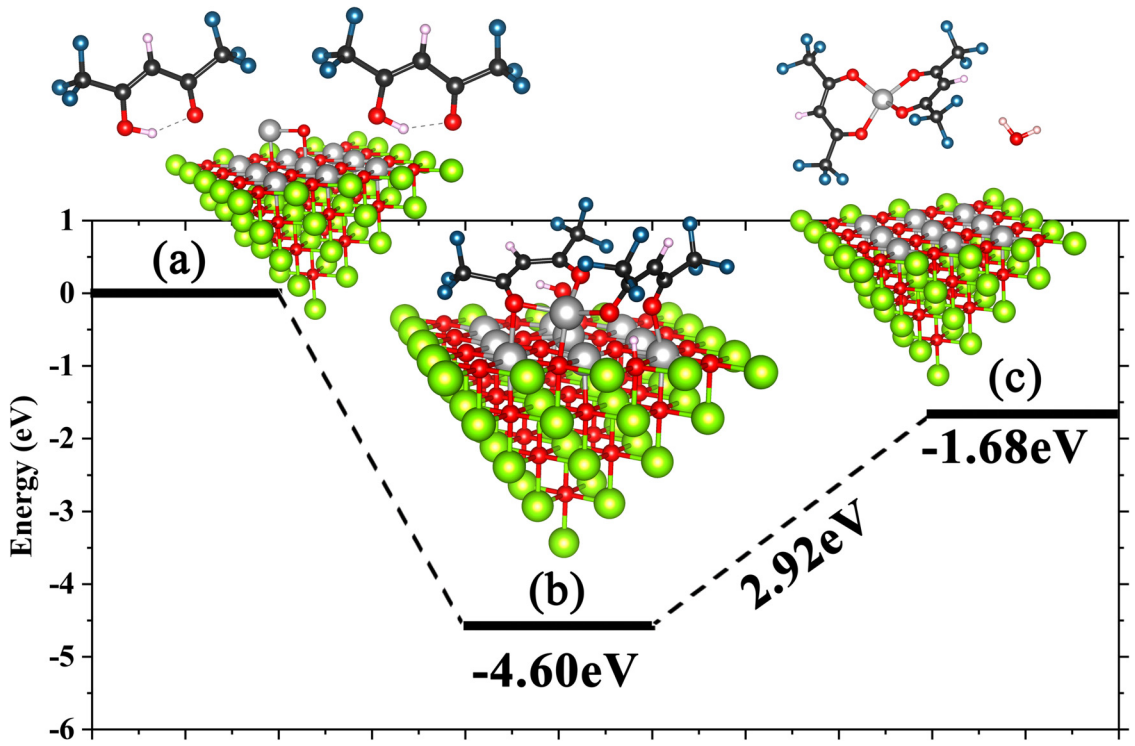

FIG. 10. System energies of different states of atomic configurations. The initial state prior to the adsorption of two hfacH molecules on the rough surface of Fig. 3(a) is depicted in (a), where the system energy is set to be zero. The state of two hfacH molecules adsorbed on the surface [i.e., Fig. 8(a)] is shown in (b). The final state where both an H_2O molecule and a $Ni(hfac)_2$ complex have desorbed from the surface is depicted in (c). The structural optimization among all Ni, O, C, F, and H atoms was performed for each state.

molecule(s) prior to the interaction, and E_{surf} is the total energy of the surface material model prior to the interaction, all after structural optimization.

We studied the adsorption of an hfacH molecule on the model surface of Fig. 2(a) by placing an hfacH molecule at various positions just above the model surface near its center and performing the structural optimization of the entire system. The structural optimization was performed with the positions of all Mg and PCs being fixed, as described in Sec. II. Prior to structural optimization, the hfacH molecule was placed vertically to the surface with its two O atoms closest to the surface. The two O atoms were positioned at equal distances from the (100) surface.

Upon obtaining converged calculation, we observed that the hfacH molecule was deprotonated by transferring its H atom to one of the surface O atoms in a barrierless process, which is in agreement with the earlier study.[1] Among various adsorption sites examined in this study, the most stable configuration of an hfacH adsorbed surface is shown in Fig. 5, where an $hfac^-$ anion is found to be stabilized with its two O atoms being bonded with two adjacent Ni atoms of the top surface. The reaction energy of this adsorption process was found to be −2.26 eV. The reaction energy of the same adsorption process evaluated with the six shell model of Fig. 2(b) was found to be −2.08 eV. The same calculations were also performed with two other exchange-correlation functionals, namely, PBE0[56] and B3LYP[57–62] and the same basis sets, including or excluding dispersion corrections D3 with BJ damping, for the four shell model of Fig. 2(a). These results are summarized in Table II. In Fig. 5, the tilted angle of the hexafluoroacetylacetonate (hfac) group measured from the normal direction of the (100) surface is 52°. (The Mulliken charge distribution of Fig. 5 is provided as Fig. S1,[63] which shows that the negatively charged O atoms of the deprotonated hfacH are bonded with positively charged Ni atoms on the surface, as discussed in the earlier study.[1])

Although a hybrid exchange-correlation functional B3LYP is considered more accurate in evaluating valence orbitals of transitions metals and their oxides,[57–59,61] it typically requires much more computational time than PBE, whereas, as seen in Table II, the calculated energies by all three functionals are within a relative deviation of 10%. Therefore, in this study, we use PBE for our DFT calculations unless otherwise indicated. Since our goal is not to pursue a highly accurate energy evaluation, we are content with a single decimal approximation to the energy level (in eV units) obtained in this study. However, we keep up to two decimal places of all energy values obtained from our calculations in this article for the reader who may be interested in reproducing our results with the same computational method.

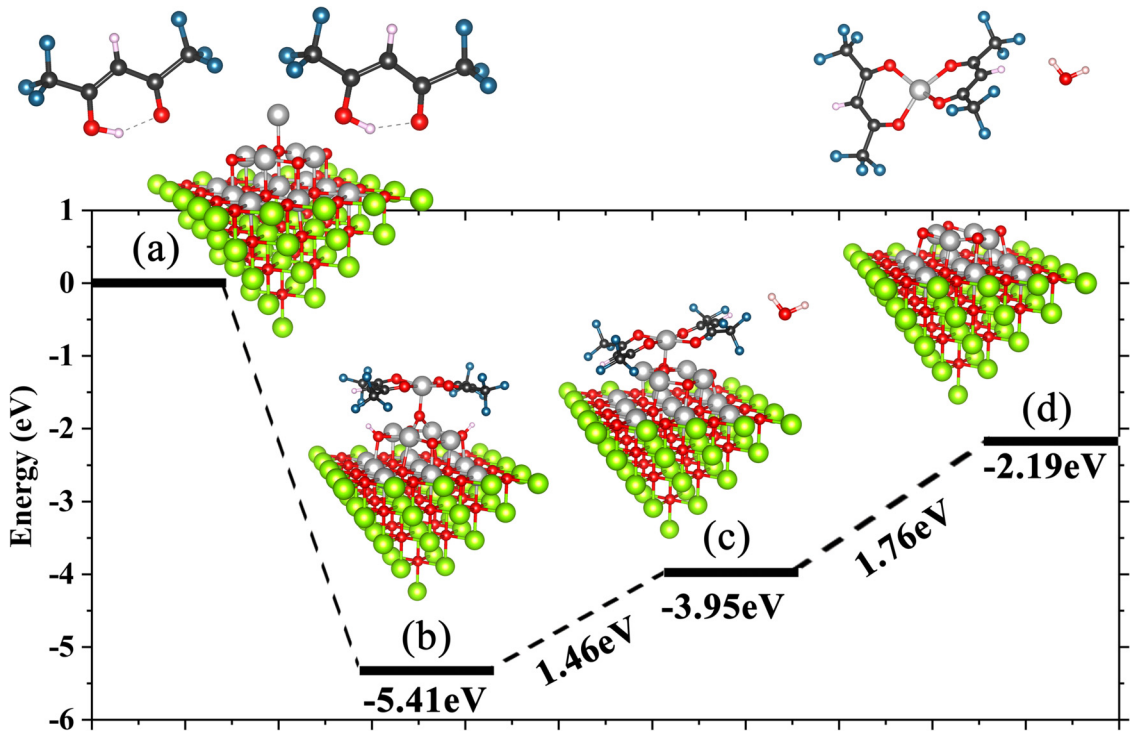

FIG. 11. System energies of different states of atomic configurations. The initial state prior to the adsorption of two hfacH molecules on the rough surface of Fig. 3(b) is depicted in (a), where the system energy is set to be zero. The state of two hfacH molecules adsorbed on the surface [i.e., Fig. 8(b)] is shown in (b). The state of H_2O molecule desorption from (b), while two hfac groups remain adsorbed on the surface is presented in (c). The final state where both an H_2O molecule and a $Ni(hfac)_2$ complex desorbed from the surface is depicted in (d). The structural optimization among all Ni, O, C, F, and H atoms was performed for each state.

As seen in Table II, the calculated reaction energies without dispersion correction D3/BJ damping are much lower in magnitude than those with dispersion correction. This clearly shows that dispersion energy accounts for a significant part (~1 eV) of the total energy for the stable absorption of deprotonated hfacH (i.e., $hfac^-$) and the proton H^+ on the NiO surface. The reaction energy obtained here is in reasonable agreement with what was reported in the earlier study.[1] Second, we examined the formation process of volatile organometallic complex $Ni(hfac)_2$ on a NiO surface. The optimized structure of a $Ni(hfac)_2$ complex is shown in Fig. 6. For this complex to be formed, two hfac groups need to bond with a single Ni atom. Therefore, we placed another hfacH molecule near the bonding site of the hfac group of Fig. 5 and performed the structural optimization of the system, which led to the atomic configuration shown in Fig. 7. The structural optimization showed that the second hfacH molecule deprotonated but two hfac groups did not bond with a single Ni atom on the surface. The reaction energy for the adsorption of these two hfacH molecules was found to be −4.20 eV. (It was found to be −4.73 eV when the B3LYP functional and same basis sets were used.) The tilting angles of the left and right hfac groups in Fig. 7 are 29° and 56°.

Despite an extensive search for an optimal position of the second hfacH molecule that could form a $Ni(hfac)_2$-like structure, we were unable to find a stable configuration of two hfac groups bonded to a single Ni atom of the flat surface. This suggests that the formation of $Ni(hfac)_2$ is unlikely to occur on the flat (100) NiO surface. The atomic configuration of Fig. 7 suggests that a geometrical interference of two hfac groups prevents them from bonding to a single Ni atom on the surface.

Rough surfaces such as those of Figs. 3(a) and 3(b) may allow two hfac groups to bond to a single Ni atom protruding from the surface without much geometrical interference. By performing structural optimization after placing two hfacH molecules near the protruding Ni atom of Fig. 3(b), we found both hfacH molecules deprotonated and three O atoms of the two hfac groups clearly bonded to the Ni atom, as seen in Fig. 8(a). The reaction energy for this adsorption process for the two hfacH molecules was found to be −4.60 eV. Similarly, the structural optimization of two hfacH molecules placed near the topmost Ni atom of Fig. 3(b) led to the atomic configuration shown in Fig. 8(b), where a $Ni(hfac)_2$-like structure is clearly seen to be formed, although its Ni atom is still bonded with an O atom of the surface. Its reaction energy was found to be −5.41 eV.

The minimum energy required to desorb a $Ni(hfac)_2$ complex and a water molecule H_2O from each atomic configuration of Fig. 8 was also evaluated. Figure 9 shows how the system energy changes

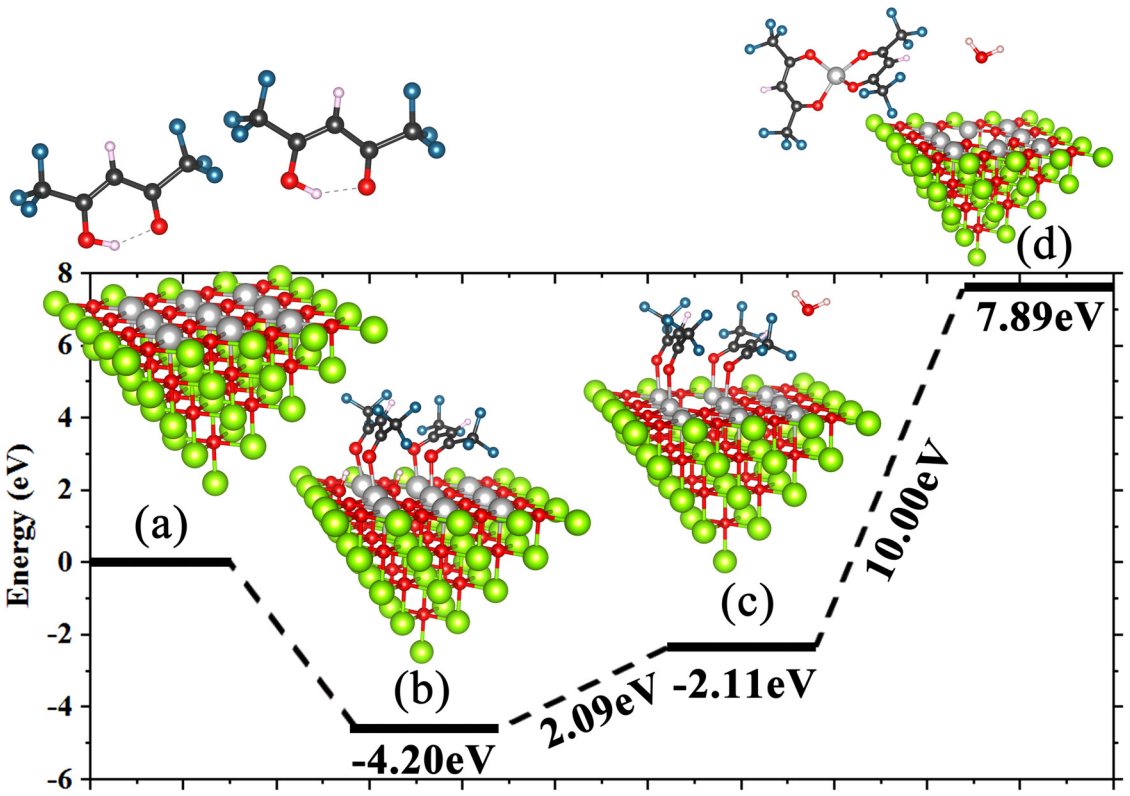

FIG. 12. System energies of different states of atomic configurations. The initial state prior to the adsorption of two hfacH molecules on the Ni (100) surface of Fig. 2(a) is depicted in (a), where the system energy is set to be zero. The state of two hfacH molecules adsorbed on the surface (i.e., Fig. 7) is shown in (b). The state of H_2O molecule desorption from (b), while two hfac groups remain adsorbed on the surface is presented in (c). The final state where both an H_2O molecule and a $Ni(hfac)_2$ complex desorbed from the surface is depicted in (d). The structural optimization among all Ni, O, C, F, and H atoms was performed for each state.

if the Ni atom bonded with two hfac groups is detached from the surface in the vertical direction, where the black and red curves show the cases of Figs. 8(a) and 8(b). The abscissa represents the distance of the Ni atom measured from its original position given in Fig. 8. The ordinate represents the change in the system energy. In this approach, only the Ni atom in the center, surrounded by the two hfac groups, was moved stepwise vertically in the upward direction, where structural optimization was performed for the rest of the atoms, including those of hfac groups, in each step. (In the surface material model, all Mg atoms and PCs were immobile during optimization, as stated before.) It is seen that the system energy increases monotonically until $Ni(hfac)_2$ desorbs completely from the surface. (Note that the H atoms are still on the surface.) The energy required for the complete isolation of $Ni(hfac)_2$ from the surface is the desorption energy, which is 3.81 eV for the system in Fig. 8(a) and 2.97 eV for the system in Fig. 8(b).

Figure 10 depicts the difference in system energy among each atomic configuration when the rough surface of Fig. 3(a) is exposed to two hfacH molecules. The total energy prior to adsorption is set to be zero (a). As given in Fig. 8(a), the adsorption energy for two hfacH molecules on the surface is −4.60 eV (b). After both an organometallic complex $Ni(hfac)_2$ and a water molecule H_2O desorb from the surface, as illustrated in (c), the system energy becomes −1.68 eV, which makes the energy difference between the adsorbed and desorbed states 2.93 eV. As discussed earlier, the structural optimization was performed in the prescribed manner for all atomic configurations shown in Fig. 10.

Similarly, Fig. 11 depicts the difference in system energy among each atomic configuration when the rough surface of Fig. 3(b) is exposed to two hfacH molecules. The total energy prior to adsorption is set to be zero (a), as in Fig. 10. As given in Fig. 8(b), the adsorption energy of two hfacH molecules on the surface was −5.41 eV (b). After a water molecule desorbs from the surface, as illustrated in (c), the system energy becomes −3.95 eV. After both organometallic complex $Ni(hfac)_2$ and water molecule H_2O desorb from the surface, as illustrated in (d), the system energy becomes −2.19 eV. Although we have not evaluated the activation energy from one state to another, the energy diagram of Fig. 11 suggests that such stepwise desorption may take place at an elevated surface temperature. (The energy diagram of Fig. 10 including a similar H_2O desorption state is provided as supplementary material.[63])

To demonstrate the difficulty of removing Ni and O atoms from the flat (100) surface, we also present the energy diagram in Fig. 12 for the case of Fig. 7. The total energy prior to adsorption is set to be zero (a), as in the previous figures. As discussed earlier, the adsorption energy for two hfacH molecules on the Ni (100) surface is −4.20 eV (b). Although we have stated that the formation of Ni $(hfac)_2$ on this surface is very unlikely, we can evaluate the energy levels of desorbed states. The energy levels of desorption of an H_2O molecule only (c) and both desorption and both $Ni(hfac)_2$ and H_2O (d) are −2.11 and 7.89 eV. Because the energy gap between (c) and (d) is 10 eV, the direct transition from the adsorption of hfacH to the desorption of $Ni(hfac)_2$ on the flat surface is very unlikely even at an elevated surface temperature of ~300–400 °C.

IV. SUMMARY AND CONCLUSIONS

We have examined stable adsorption of hfacH molecules on a NiO (100) surface and possible formation of volatile organo-nickel complexes $Ni(hfac)_2$ and water molecules H_2O from the surface at elevated surface temperature, using DFT calculations. This study uses a more realistic extended NiO surface model larger than the model surface used in the earlier study.[1] We have confirmed in the new calculations that, when an hfacH molecule approaches a NiO (100) surface, it deprotonates barrierlessly and the negatively charged O atoms of the deprotonated $hfac^-$ anion bond with positively charged Ni atoms of the surface. The nature of ionic bonds (i.e., the charge distribution) of a metal oxide surface promotes the deprotonation and adsorption of hfacH molecules. The adsorption mechanism and adsorption energy of an hfacH molecule on a NiO (100) surface obtained in this study are consistent with what was reported in the earlier study.[1]

We have also examined how two hfacH molecules adsorbed on a NiO surface can form a $Ni(hfac)_2$ complex at an elevated surface temperature. On a flat NiO (100) surface, two hfacH molecules can deprotonate and adsorb barrierlessly. However, we were unable to find a (meta)stable configuration where two hfac groups bonded to a single Ni atom of the NiO surface. It seems such a configuration is unstable and two hfac groups tend to bond with different Ni atoms on the surface. This indicates that the formation of a $Ni(hfac)_2$ complex on the flat surface is very unlikely.

In the case of a rough NiO surface, some Ni atoms may protrude over their surrounding atoms and allow two hfac groups to bond to a single Ni atom without much geometrical interference. Models of rough NiO surfaces examined in this study are those given in Figs. 3(a) and 3(b). In each case, the topmost Ni atom is under-coordinated and has enough space around it to capture two hfac groups stably after both hfacH molecules deprotonated, as shown in Fig. 8. In other words, our DFT calculations have demonstrated that roughness of a NiO surface can promote the formation of organo-nickel complexes $Ni(hfac)_2$ on its surface. In earlier experiments,[20,24] volatile $Ni(hfac)_2$ and H_2O desorb from the surface at a temperature of around 300 °C or higher. In the case of Fig. 11, the required energy for complete desorption to occur from the adsorbed state is less than 2.0 eV in each step. A more quantitative study on the relation between the energy diagrams of Figs. 10–12 and experimental observation of desorption is the subject of a future study.

Our study indicates that in a thermal ALE process of metal consisting of an oxidation step and a removal step aided by the formation of volatile organometallic complexes, the surface roughness incidentally caused by the oxidation step may play a critical role in enhancing the thermal desorption rate of organometallic complexes in the subsequent removal step. If protruding metal atoms are preferentially removed from the surface in the desorption step, the surface roughness decreases and so may the desorption rate. In other words, thermal ALE of this type for a rough metal surface tends to increase its smoothness. This is consistent with experimental observations of surface smoothing in a similar thermal ALE process of cobalt (Co) consisting of surface chlorination steps and removal steps of the chlorinated Co layers by hfacH at elevated surface temperature, as reported in Refs. 23 and 26. As pointed out by Kanarik *et al.*,[10] the smoothing effect seems to be an intrinsic characteristic also of thermal ALE of this type.

Our results also indicate that the etching of a metal oxide by the formation and thermal desorption of organometallic complexes should be slower or may even hardly proceed for a crystalline metal oxide compared with an amorphous or microcrystalline metal oxide. This is because the latter has more under-coordinated metal atoms near the surface or on the grain boundaries, which are more likely to interact with incident organic molecules and form organometallic complexes.

This study focused on the adsorption and desorption reactions taking place on an oxidized metal surface in a thermal ALE using organic molecules. However, it does not explain why the etching process ceases when a metal surface reappears after the oxidized layer is completely removed. (Therefore, the etching process is called self-limiting.) The earlier study[1] indicates that hfacH molecules do not deprotonate and tend to decompose on a metallic Ni surface. In the same line with this study, DFT calculations of interactions between incident hfacH molecules and a metallic Ni surface using a more realistic extended surface model than that used in Ref. 1 are desirable for a better theoretical understanding of the thermal ALE process. The results of such a study are deferred to a future publication.

ACKNOWLEDGMENTS

A.H.B. appreciates support from Professional Development Consortium for Computational Materials Scientists (PCoMS), which allowed him to visit M.K. and W.W. at Karlsruhe Institute of Technology (KIT), Germany, during this study. The authors are also grateful to Pascal Friederich of KIT for fruitful discussion. This work was partially supported by the Japan Society for the Promotion of Science (JSPS) Grants-in-Aid for Scientific Research (S) No. 15H05736, JSPS Core-to-Core Program No. JPJSCCA2019002, and Deutsche Forschungsgemeinschaft (DFG, German Research Foundation) under Germany's Excellence Strategy—Nos. 2082/1–390761711 and GRK 2450.

REFERENCES

[1] A. H. Basher, M. Krstić, T. Takeuchi, M. Isobe, T. Ito, M. Kiuchi, K. Karahashi, W. Wenzel, and S. Hamaguchi, J. Vac. Sci. Technol. A **38**, 022610 (2020).
[2] G. S. Oehrlein and S. Hamaguchi, Plasma Sources Sci. Technol. **27**, 023001 (2018).

[3]G. Yuan, N. Wang, S. Huang, and J. Liu, "A brief overview of atomic layer deposition and etching in the semiconductor processing," *2016 17th International Conference on Electronic Packaging Technology*, Wuhan, Hubei, China, 16–19 August 2016 (ICEPT, Wuhan, 2016), pp. 1365–1368.
[4]D. Metzler, R. L. Bruce, S. Engelmann, E. A. Joseph, and G. S. Oehrlein, J. Vac. Sci. Technol. A **32**, 020603 (2014).
[5]S. M. George, Chem. Rev. **110**, 111 (2010).
[6]A. Agarwal and M. J. Kushner, J. Vac. Sci. Technol. A **27**, 37 (2009).
[7]S. Rauf, T. Sparks, P. L. G. Ventzek, V. V. Smirnov, A. V. Stengach, K. G. Gaynullin, and V. A. Pavlovsky, J. Appl. Phys. **101**, 033308 (2007).
[8]A. Fischer, A. Routzahn, Y. Lee, T. Lill, and S. M. George, J. Vac. Sci. Technol. A **38**, 022603 (2020).
[9]K. J. Kanarik, T. Lill, E. A. Hudson, S. Sriraman, S. Tan, J. Marks, V. Vahedi, and R. A. Gottscho, J. Vac. Sci. Technol. A **33**, 020802 (2015).
[10]K. J. Kanarik, S. Tan, and R. A. Gottscho, J. Phys. Chem. Lett. **9**, 4814 (2018).
[11]P. C. Lemaire and G. N. Parsons, Chem. Mater. **29**, 6653 (2017).
[12]M. A. George, D. W. Hess, S. E. Beck, K. Young, D. A. Bohling, G. Voloshin, and A. P. Lane, J. Electrochem. Soc. **143**, 3257 (1996).
[13]T. Matsuura, J. Murota, Y. Sawada, and T. Ohmi, Appl. Phys. Lett. **63**, 2803 (1993).
[14]Y. Aoyagi, K. Shinmura, K. Kawasaki, T. Tanaka, K. Gamo, S. Namba, and I. Nakamoto, Appl. Phys. Lett. **60**, 968 (1992).
[15]P. Walker and W. H. Tarn, *Handbook of Metal Etchants* (CRC, Boca Raton, FL, 1991).
[16]Y. Horiike, T. Tanaka, M. Nakano, S. Iseda, H. Sakaue, A. Nagata, H. Shindo, S. Miyazaki, and M. Hirose, J. Vac. Sci. Technol. A **8**, 1844 (1990).
[17]M. N. Yoder, U.S. Patent 4,756,794 (12 July 1988).
[18]C. T. Carver, J. J. Plombon, P. E. Romero, S. Suri, T. A. Tronic, and R. B. Turkot, ECS J. Solid State Sci. Technol. **4**, N5005 (2015).
[19]W. Boullart, D. Radisic, V. Paraschiv, S. Cornelissen, M. Manfrini, K. Yatsuda, E. Nishimura, T. Ohishi, and S. Tahara, Proc. SPIE **8685**, 86850F (2013).
[20]H. L. Nigg and R. I. Masel, J. Vac. Sci. Technol. A **17**, 3477 (1999).
[21]Y. Lee and S. M. George, J. Phys. Chem. C **123**, 18455 (2019).
[22]S. M. George and Y. Lee, ACS Nano **10**, 4889 (2016).
[23]J. Zhao, M. Konh, and A. V. Teplyakov, Appl. Surf. Sci. **455**, 438 (2018).
[24]T. Ito, K. Karahashi, and S. Hamaguchi, in Proceedings of the 39th International Symposium on Dry Process, Tokyo, Japan, 16–17 November 2017, Vol. E-4, p. 45.
[25]A. I. Abdulagatov and S. M. George, J. Vac. Sci. Technol. A **38**, 022607 (2020).
[26]M. Konh, C. He, X. Lin, X. Guo, V. Pallem, R. Opila, A. Teplyakov, Z. Wang, and B. Yuan, J. Vac. Sci. Technol. A **37**, 021004 (2019).
[27]J. K. Chen, N. D. Altieri, T. Kim, E. Chen, T. Lill, M. Shen, and J. P. Chang, J. Vac. Sci. Technol. A **35**, 05C305 (2017).
[28]J. K. Chen, T. Kim, N. D. Altieri, E. Chen, and J. P. Chang, J. Vac. Sci. Technol. A **35**, 031304 (2017).
[29]TURBOMOLE V7.3.1 2018, a development of University of Karlsruhe and Forschungszentrum Karlsruhe GmbH, 1989–2007, TURBOMOLE GmbH, since 2007; see: http://www.turbomole.com
[30]H. Li *et al.*, J. Vac. Sci. Technol. A **35**, 05C303 (2017).
[31]K. Fink, J. Phys. Chem. Chem. Phys. **7**, 2999 (2005).
[32]V. Butera and M. C. Toroker, Materials **10**, 480 (2017).
[33]V. E. Henrich and P. A. Cox, *The Surface Science of Metal Oxides* (Cambridge University, Cambridge, 1994).
[34]S. Nakagomi, T. Yasuda, and Y. Kokubun, Phys. Status Solidi B **257**, 1900669 (2019).
[35]K. Persson, Materials Data on NiO (SG:225) by Materials Project. United States: N. P., 2014.
[36]T. Archer *et al.*, Phys. Rev. B **84**, 115114 (2011).
[37]D. Ködderitzsch, W. Hergert, W. M. Temmerman, Z. Szotek, A. Ernst, and H. Winter, Phys. Rev. B **66**, 064434 (2002).
[38]J. Tao, J. P. Perdew, V. N. Staroverov, and G. E. Scuseria, Phys. Rev. Lett. **91**, 146401 (2003).
[39]J. P. Perdew, K. Burke, and M. Ernzerhof, Phys. Rev. Lett. **78**, 1396 (1997).
[40]J. P. Perdew, K. Burke, and M. Ernzerhof, Phys. Rev. Lett. **77**, 3865 (1996).
[41]J. P. Perdew and Y. Wang, Phys. Rev. B **45**, 13244 (1992).
[42]A. Schäfer, H. Horn, and R. Ahlrichs, J. Chem. Phys. **97**, 2571 (1992).
[43]F. Weigend, M. Häser, H. Patzelt, and R. Ahlrichs, Chem. Phys. Lett. **294**, 143 (1998).
[44]S. Grimme, S. Ehrlich, and L. Goerigk, Theory. J. Comput. Chem. **32**, 1456 (2011).
[45]S. Grimme, J. Antony, S. Ehrlich, and H. Krieg, J. Chem. Phys. **132**, 154104 (2010).
[46]E. R. Johnson and A. D. Becke, J. Chem. Phys. **123**, 024101 (2005).
[47]F. Weigend and A. Baldes, J. Chem. Phys. **133**, 174102 (2010).
[48]K. Eichkorn, F. Weigend, O. Treutler, and R. Ahlrichs, Theor. Chem. Acc. **97**, 119 (1997).
[49]K. Eichkorn, O. Treutler, H. Öhm, M. Häser, and R. Ahlrichs, Chem. Phys. Lett. **242**, 652 (1995).
[50]M. Sierka, A. Hogekamp, and R. Ahlrichs, J. Chem. Phys. **118**, 9136 (2003).
[51]H. Kung and A. Teplyakov, J. Catalysis **330**, 145 (2015).
[52]D. L. Howard, H. G. Kjaergaard, J. Huang, and M. Meuwly, J. Phys. Chem. A **119**, 7980 (2015).
[53]S. Engmann, B. Ómarsson, M. Lacko, M. Stano, Š. Matejcík, and O. Ingólfsson, J. Chem. Phys. **138**, 234309 (2013).
[54]K. Manbeck, N. Boaz, N. Bair, A. Sanders, and A. Marsh, J. Chem. Educ. **88**, 1444 (2011).
[55]M. da Silva, L. Santos, and E. Giera, J. Chem. Thermodyn. **39**, 361 (2007).
[56]M. Ernzerhof and G. E. Scuseria, J. Chem. Phys. **110**, 5029 (1999).
[57]P. Verma and D. G. Truhlar, Theor. Chem. Acc. **135**, 182 (2016).
[58]P. J. Stephens, F. J. Devlin, C. F. Chabalowski, and M. J. Frisch, J. Phys. Chem. **98**, 11623 (1994).
[59]S. H. Vosko, L. Wilk, and M. Nusair, Can. J. Phys. **58**, 1200 (1980).
[60]V. Vetere, C. Adamo, and P. Maldivi, Chem. Phys. Lett. **325**, 99 (2000).
[61]C. Lee, W. Yang, and R. G. Parr, Phys. Rev. B **37**, 785 (1988).
[62]A. D. Becke, J. Chem. Phys. **98**, 5648 (1993).
[63]See supplementary material at https://doi.org/10.1116/6.0000293 for the Mulliken partial charge distribution state of Fig. 5 and the energy diagram of Fig. 10 including a similar H_2O desorption state.